communications earth & environment

Article

https://doi.org/10.1038/s43247-024-01734-8

Winter snowpack loss increases warm-season compound hot-dry extremes

Hao Liu [1], Pengfeng Xiao [1,2] ✉, Xueliang Zhang[1], Yongxiao Liang[3], Bo Tang[1], Siyong Chen[1] & Yantao Liu[1]

Ongoing warming intensifies snowpack extremes, posing significant hydroclimatic risks to socio-ecological systems. However, the relation between snowpack extremes and subsequent compound hydroclimatic extremes remains unclear. Here, we investigated the impact of snowpack extremes on warm-season compound hydroclimatic extremes in the Northern Hemisphere using multisource datasets from 1980 to 2022. We found widespread increases in deficient, short, and deficient-short snowpack extremes, triggering more compound hot-dry extremes within a month after snowpack disappearance (mean coincidence rate over 0.6, $p < 0.05$). The impact of compound snowpack extremes exceeded that of individual snowpack extremes in both areas (over 10%) and coincidence rates (over 0.2). Meanwhile, increased intensity, rather than frequency, of snowpack extremes drove mainly the occurrence of compound hydroclimatic extremes. Furthermore, background climate factors, followed by vegetation, topography, and soil, affected relations between snowpack and compound hydroclimatic extremes. These findings will deepen our understanding of the emerging consecutive extremes and improve their predictability.

Seasonal snowpack is an important component of the Northern Hemisphere land surface, which covers nearly 50% of areas (~4.5×10^7 km^2) in winter[1] and plays a crucial role in radiative (e.g. cooling effects) and hydrological processes (water availability)[2]. In recent decades, snowpack has undergone substantial changes[3–5], raising concerns about snowpack-related hydroclimatic extremes such as droughts[6,7], heatwaves[8,9], and floods[10,11]. These extremes have caused massive damage to humans and ecosystems, such as the 2010 summer heatwave in western Russia (dwindling snowpack reduced early summer soil moisture as one of the main causes), which caused ~15,000 deaths and ~54% loss of annual vegetation productivity[12]. According to the latest Intergovernmental Panel on Climate Change (IPCC) assessment, many regions are expected to experience an increase in snowpack-related hydroclimatic extremes under climate warming, particularly for compound extremes (i.e., an extreme impact that combines multiple variables or events)[13]. Therefore, understanding the interaction between snowpack and hydroclimatic extremes is vital for reducing socio-economic losses and developing climate mitigation strategies.

Previous studies have explored the relations between snowpack and individual hydroclimatic extremes at global and regional scales. For example, ~35% of snow droughts triggered heatwaves in 7% of global snow-dominated regions from 1981 to 2020[14]. Meanwhile, the hydroclimatic consequences of snow droughts differ depending on their causes[10,15]; in western North America, warm snow droughts (temperature-driven snow deficit) typically increase the winter runoff peak, whereas dry snow droughts (precipitation-driven) reduce the annual runoff peak[16]. Moreover, changes in snowpack phenology have significant impacts on hydroclimatic events, such that extremely early snowmelt and short snow duration seasons lead to spring flooding[17,18] and rapid spring warming[19], respectively. Besides influencing individual hydroclimatic extremes, snowpack extremes result in considerable impacts on compound hydroclimatic extremes, yet these impacts remain relatively unexplored. This oversight could lead to an underestimation of the associated hydroclimatic risks.

In fact, most hydroclimatic extremes did not appear alone but rather through the interaction of different meteorological variables (i.e. compound extremes)[20], which were generally more severe than individual extremes[21,22]. Investigating whether and how abnormal snowpack changes affect compound hydroclimatic extremes, both qualitatively and quantitatively, is essential for achieving the Sustainable Development Goals[23], notably for coping with climate change and its impacts (Goal 13). Furthermore, different characteristics (e.g. mass and duration) of snowpack are coupled[24], and this dependence structure may amplify the impact of snowpack events[25]. Although univariate analyses of snowpack changes have become

[1]Jiangsu Provincial Key Laboratory of Geographic Information Science and Technology, Key Laboratory for Land Satellite Remote Sensing Applications of Ministry of Natural Resources, School of Geography and Ocean Science, Nanjing University, Nanjing, Jiangsu, China. [2]Jiangsu Center for Collaborative Innovation in Geographical Information Resource Development and Application, Nanjing, Jiangsu, China. [3]Climate Research Division, Environment and Climate Change Canada, Victoria, British Columbia, Canada. ✉e-mail: xiaopf@nju.edu.cn

widespread, the bivariate impacts of snowpack changes are still unclear, especially for extreme changes, and their evolution at a hemispheric scale has not been fully elucidated. Additionally, the differences in both spatiotemporal patterns and hydroclimatic consequences between individual and compound snowpack extremes remain unexamined, which greatly limits our in-depth understanding of climate changes. In light of the expected increase in climate change[26], it is necessary to consider changes in different snowpack characteristics simultaneously for a more realistic evaluation of snowpack hydroclimatic impacts.

Here, we aimed to investigate the impact of different snowpack extremes (rich, deficient, long, short, rich-long, rich-short, deficient-long, and deficient-short) on warm-season compound hydroclimatic extremes (several months after snowpack disappearance) in the Northern Hemisphere from 1980 to 2022 using multisource datasets. Specifically, the following four questions were addressed: (1) What are the spatiotemporal trends in the occurrence probability and intensity of different snowpack extremes? (2) How do four frequently encountered compound hydroclimatic extremes (hot-dry, hot-wet, cold-dry, and cold-wet) respond to different snowpack extremes? (3) Are compound hydroclimatic extremes more influenced by changes in the occurrence probability or intensity of snowpack extremes? (4) What are the main environmental factors driving the relations between snowpack extremes and compound hydroclimatic extremes? These results will improve our comprehensive understanding of the hydroclimatic consequences of different snowpack extremes, with implications for better predicting and mitigating the impact of future consecutive extremes on socio-ecological systems.

Results

Recent widespread increase in the occurrence and intensity of deficient, short, and deficient-short snowpack extremes

We first examined the spatiotemporal trends in the occurrence probability and intensity of different snowpack extremes over the past four decades based on a 15-year moving window using the Theil-Sen and Mann–Kendall methods (Fig. 1a–h). Eight types of snowpack extremes (rich, deficient, long, short, rich-long, rich-short, deficient-long, and deficient-short) were identified by using snow water equivalent and snowpack duration indices based on the bivariate copula function. The rich/deficient snowpack extremes referred to high/low-level snowpack mass, and long/short snowpack extremes referred to high/low-level snowpack duration (see "Methods" for details).

Most snowpack extremes showed significant changes and great spatial heterogeneity across the Northern Hemisphere's seasonal snow-dominated regions (Fig. 1g, h), except for less frequent deficient-long and rich-short snowpack extremes (Supplementary Fig. 1). Specifically, the deficient, short, and deficient-short snowpack extremes presented significant increasing trends in both occurrence probability and intensity, with areas of change ($p < 0.05$) accounting for 27%, 38% and 27% of the study area, respectively. High increasing trends occurred in Inner Eurasia, such as in the Siberian region, with some scattered trends occurring in the mid-to-high latitudes of North America. In contrast, the occurrence probability and intensity of rich, long, and rich-long snowpack extremes mainly exhibited significant decreasing trends, which were more pronounced for occurrence probability changes, with areas of changes ($p < 0.05$) accounting for 19%, 34%, and 24% of the study area, respectively. Hotspots of significant decreasing trends (over 0.05 yr^{-1}) in both occurrence probability and intensity of long snowpack extremes occurred mainly in the Eastern European Plain and most of the Siberian regions, while those of rich and rich-long snowpack extremes were distributed mainly in the mid-latitude regions of Europe (~50°N) and northern Russia regions. Additionally, the robustness of the temporal results was examined via 13-year and 17-year moving windows (Supplementary Fig. 2 and Fig. 3), and the spatial pattern of trends in snowpack extremes obtained was consistent with that obtained via the 15-year moving window.

High coincidence rate of snowpack extremes with compound hydroclimatic extremes

By analyzing the four compound hydroclimatic extremes monthly during the warm season (Fig. 2a), with a focus on five potential impact lags (1–5 months) after snowpack end date, we found that compound hot-dry and cold-wet extremes were more closely related to snowpack extremes based on coincidence analysis (see "Methods"). Notably, compound snowpack extremes (deficient-short and rich-long) had greater impacts on hydroclimatic extremes than individual snowpack extremes alone. The impact differences were apparent in both spatial extent and significant coincidence rates (i.e., the occurrence probability of compound hydroclimatic extremes after snowpack extremes), with compound hot-dry extremes showing average increases of 10% and 0.2 ($p < 0.05$) and with compound cold-wet extremes showing average increases of 2% and 0.15, respectively. In view of the above, the following analyses focus primarily on the hydroclimatic impact of deficient-short and rich-long snowpack extremes.

Specifically, the significant coincidence rate between deficit-short snowpack extremes and compound hot-dry extremes (DS&HD) was highest in the month after snowpack disappearance (mean of ~0.79), and the area proportion decreased with increasing lag time, ranging from 15.7% to 2% of the study area (Fig. 2b, d). Similarly, these phenomena were observed in the relation between rich-long snowpack extremes and compound cold-wet extremes (RL&CW; Fig. 2c, e). Spatially, snowpack extremes had a clustering impact on compound hydroclimatic extremes, and their coincidence rates presented large heterogeneity. The successive DS&HD events mainly occurred in regions such as eastern Europe, Siberia, and mid-to-high latitudes of North America. In comparison, the significant coincidence rate of RL&CW was relatively low (mean of ~0.62) and scattered, with highly significant coincidence rates mainly found in western North America and western Siberia.

Moreover, snowpack extremes could influence hydrothermal conditions in neighboring regions, potentially leading to the co-occurrence of hydroclimatic extremes in different regions. We further analyzed spatial distance scales of the co-occurrence rate of compound hydroclimatic extremes caused by snowpack extremes at the pixel scale (see "Methods"). In general, the magnitude and area proportion of co-occurrence rates decreased with increasing distance scale for both DS&HD and RL&CW events (Fig. 2f, g), suggesting the local nature of the hydroclimatic impact of snowpack extremes. The spatial co-occurrence rates were less than 0.1 for DS&HD and RL&CW events when the distance between pixels exceeded ~800 km and ~600 km, respectively. Additionally, we found that the distance of the co-occurrence rate of compound hydroclimatic extremes resulting from snowpack extremes followed an "∩" shape, increasing and then decreasing with increasing latitude.

An increased intensity of snowpack extremes amplifies compound hydroclimatic extremes

Understanding whether the significant coincidence rate between compound hydroclimatic extremes and snowpack extremes is related to the high frequency, intensity, or both of snowpack extremes is critical for accurately predicting these emerging compound extremes. Consequently, we first examined the relation between the frequency of snowpack extremes and hydroclimatic extremes, and found that the number of snowpack extremes exhibited a large discrepancy with that of hydroclimatic extremes (Supplementary Fig. 4). This implied that the high frequency of snowpack extremes did not necessarily increase the occurrence of hydroclimatic extremes. We then conducted an analysis of the sensitivity of hydroclimatic extremes to the intensity of snowpack extremes. The sensitivity was calculated as the changes in hydroclimatic extremes' indices caused by a unit change in the intensity of snowpack extremes.

The results showed that two-thirds of significant regions exhibited high sensitivity (over 1) of compound hot-dry extremes to changes in the intensity of deficient-short snowpack extremes (HD to DS), with an apparent latitudinal distribution with a significant decreasing trend (–0.01, $p < 0.05$) from south to north (Fig. 3a). However, the sensitivity of

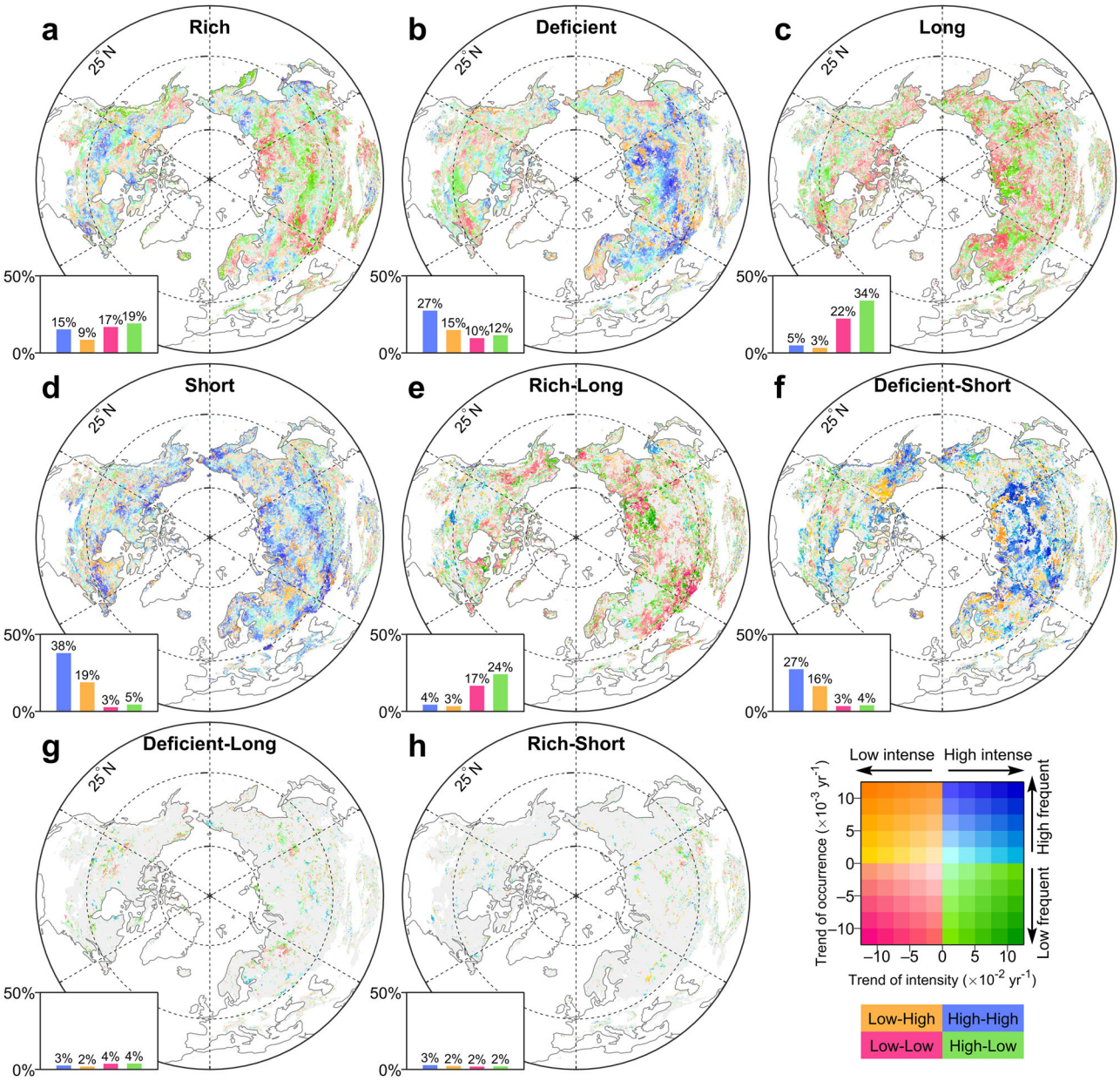

Fig. 1 | Spatial distribution of trends in the occurrence probability and intensity of different snowpack extremes from 1980 to 2022 in the Northern Hemisphere. **a**–**h** Significant trends (colored areas, $p < 0.05$) of rich, deficient, long, short, rich-long, rich-short, deficient-long, and deficient-short snowpack extremes. The gray areas indicate the seasonal snow-dominated regions in the Northern Hemisphere (i.e. the study area). The inset histograms indicate the areas exhibiting a particular trend, categorized as low-high, high-high, low-low, or high-low combinations of occurrence probability and intensity trends.

compound cold-wet extremes to the intensity of rich-long snowpack extremes (CW to RL) was relatively low and presented a significantly increasing (0.01) latitudinal gradient (Fig. 3b). Regionally, the highest mean sensitivities of HD to DS and CW to RL were observed in the CAN and RAR regions, respectively (Fig. 3c). Most regions showed greater sensitivity of HD to DS, particularly in North America and Eastern Europe, which again implied that deficient-short snowpack extremes had greater hydroclimatic consequences. Moreover, we quantified the impact of snowpack extremes' intensity on changes in coincidence rates between DS&HD and RL&CW events using the Ordinary Least Squares regression, and found a positive correlation between the intensity of snowpack extremes and their coincidence rates. A one-unit increase in the intensity of deficient-short and rich-long extreme events resulted in an increase of 0.08 and 0.03 in the coincidence rate for DS&HD and RL&CW events, respectively (Fig. 3d, e).

Strong dependence on background climate factors

Considering that background environmental factors play an important role in controlling relations between snowpack and compound hydroclimatic extremes, we further assessed the importance of four types of environmental factors (during the period 1980–2022) in regulating the coincidence rate of DS&HD and RL&CW events based on the geographical detector model (see "Methods"). Overall, climate factors contributed a large proportion (mean of ~41%) of the change in the coincidence rate between snowpack and hydroclimatic extremes, followed by vegetation factors (~33%), topography factors (~15%), and soil factors (~11%) (Fig. 4a, b). Annual mean solar radiation was the most important controlling climate variable for both DS&HD and RL&CW events and was positively associated with coincidence rate variations. Several considerably important variables, including elevation, annual mean wind, annual mean aridity index, and soil bulk density, had opposite impacts on the coincidence rate of DS&HD and

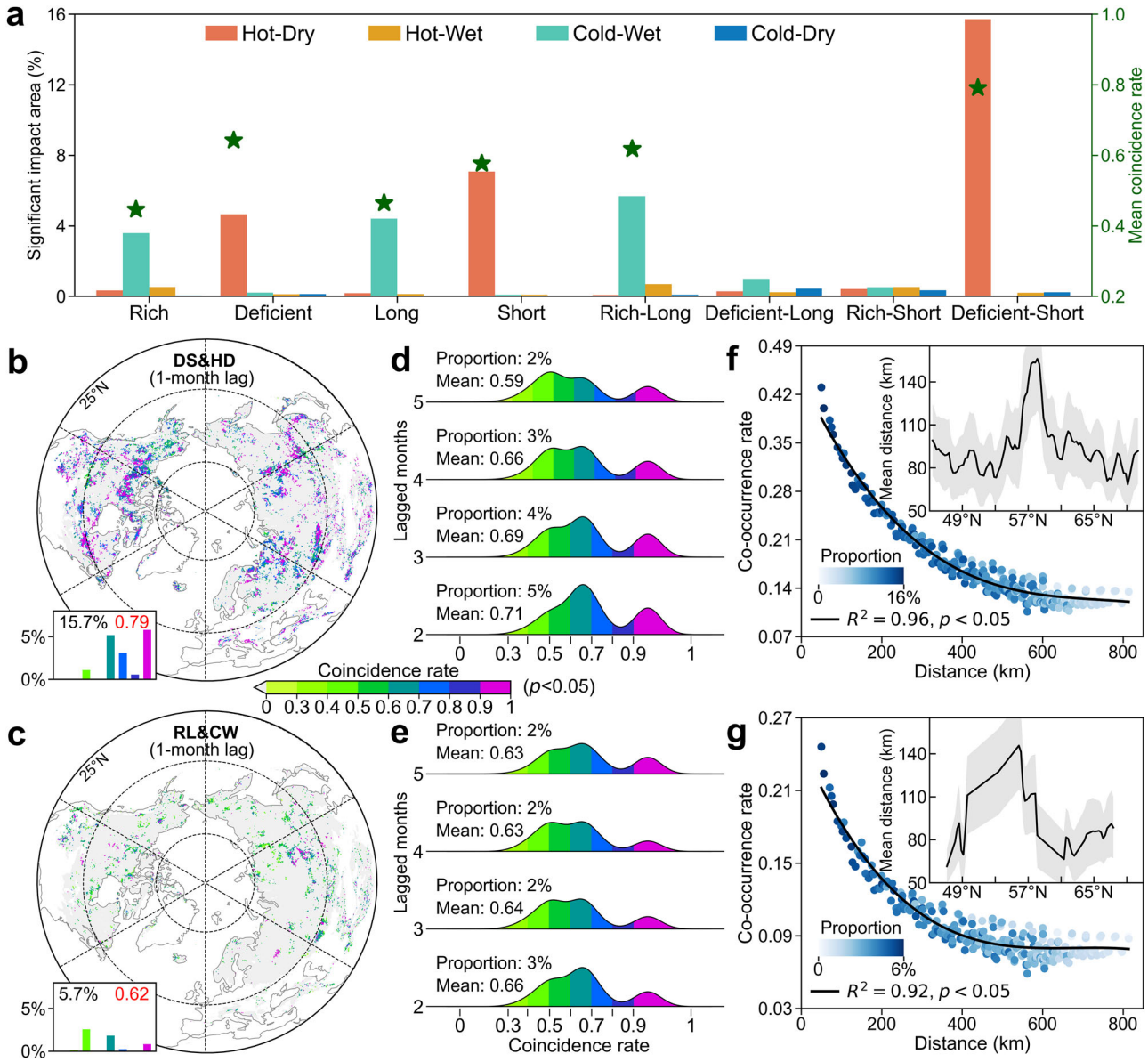

Fig. 2 | Relations between snowpack extremes and compound hydroclimatic extremes. a Maximum area proportion and magnitude of significant coincidence rates ($p < 0.05$) between different snowpack extremes and compound hydroclimatic extremes at 1–5-month lags after snowpack disappearance. The mean significant coincidence rate is only calculated for area proportions greater than 2%. **b**, **c** Spatial patterns of the significant coincidence rates (colored areas) between deficient-short snowpack extremes and compound hot-dry extremes (DS&HD) and between rich-long snowpack extremes and compound cold-wet extremes (RL&CW) at a 1-month lag. The black and red numbers in the inset histograms indicate the area proportion and mean value of significant coincidence rates, respectively. **d**, **e** Area proportion and mean value of the significant coincidence rate for DS&HD and RL&CW at 2–5-month lags. **f**, **g** Distance scales of the spatial co-occurrence rate of DS&HD and RL&CW. Each panel shows the coefficient of determination (R^2) for the fitted cubic polynomial regression. The inset plot indicates the latitudinal distribution of the spatial co-occurrence rate, and the shaded area indicates a ± 0.5 standard deviation.

RL&CW events. In comparison, topographic characteristics such as slope and aspect, depth to bedrock, and plant type had relatively minor impacts.

Furthermore, we evaluated the dominant factors contributing to changes in the coincidence rate of DS&HD and RL&CW events in different climate reference regions. The proportions of the cumulative contribution from four types of factors in different regions were generally consistent with those in the whole region, with climate factors being the main contributors (Fig. 4e), but there were differences in some regions. For example, vegetation was the most relevant factor for DS&HD events in North America (NWN and NEN) and northern Russia (RAR) (Fig. 4c). For RL&CW events, topography factors in NWN and TIB regions, vegetation factors in the RFE and WNA regions, and soil factors in the WCA region were identified as the most important drivers (Fig. 4d). Moreover, the importance of each variable varied across regions (Supplementary Figs. 5, 6), suggesting the need for specific strategies for regional hydroclimatic extremes.

Discussion

Our analysis revealed a significant increase in both the occurrence probability and intensity of deficient, short, and deficient-short snowpack extremes over the past four decades, most pronounced in Eurasia and northern North American regions (Fig. 1). These decreases in snowpack agreed with previous studies based on station-observed and model-simulated datasets[27–30]. Conversely, the occurrence probability and intensity of rich, long, and rich-long snowpack extremes mainly exhibited significant decreasing trends, particularly in terms of intensity. In addition to the trend induced by climate warming[17,31], the close relation between snowpack mass

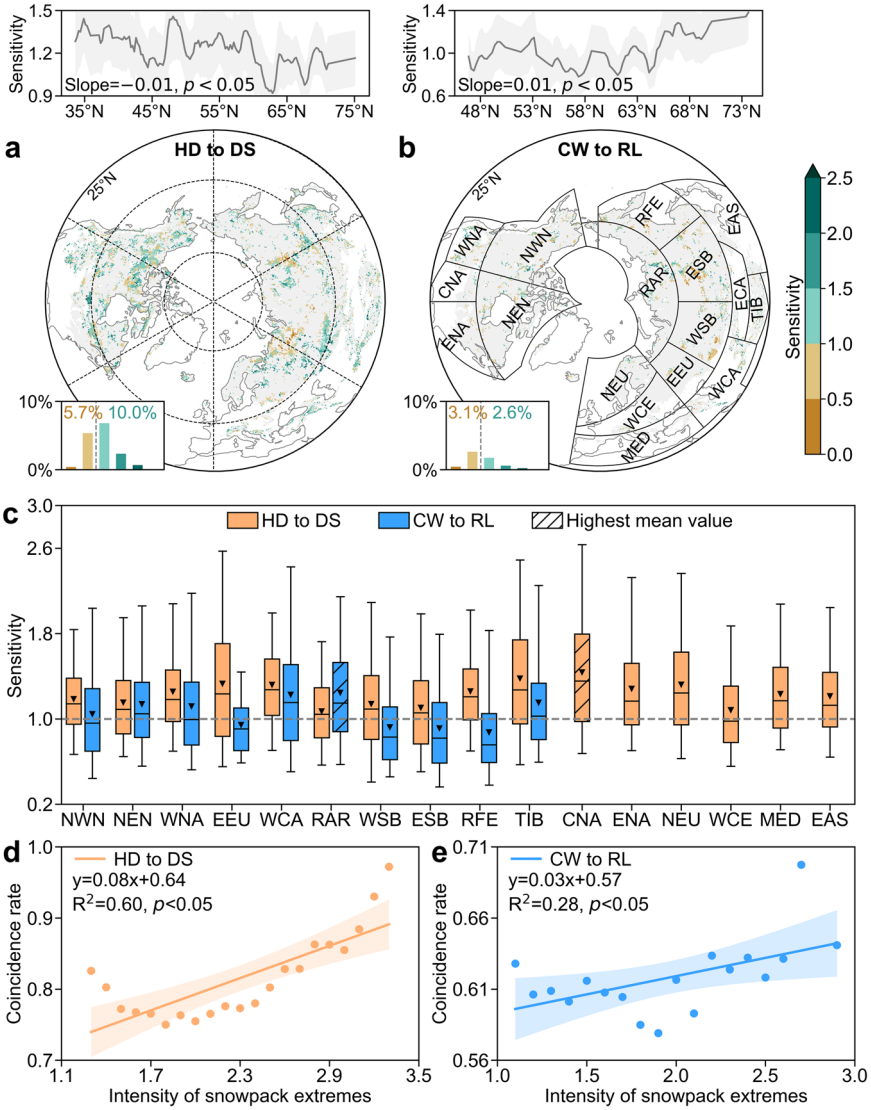

Fig. 3 | Sensitivity of compound hydroclimatic extremes to the intensity of snowpack extremes. **a**, **b** Geographical and latitudinal patterns of the sensitivity of compound hot-dry and cold-wet extremes to the intensity of deficient-short (a, HD to DS) and rich-long (b, CW to RL) snowpack extremes, respectively. The gray areas indicate the pixels with non-significant coincidence rates, and brown and green numbers in the inset histogram indicate the areas with the sensitivity above and below 1, respectively. **c** Sensitivity of HD to DS and CW to RL in different IPCC climate reference regions[78]. The mean values in the boxplot are marked by triangles, the centerlines indicate the median values, and the whiskers indicate the 5th/95th values. Only regions with more than 100 significant pixels are analyzed. **d**, **e** Impact of the intensity of snowpack extremes on the coincidence rate. Each point indicates the mean value of the coincidence rate within a specific intensity interval (0.1, each interval over 100 pixels) of snowpack extremes, with color-shaded areas indicating the 95% confidence interval.

and duration further exacerbated changes in snowpack extremes in most regions (Supplementary Fig. 7). These results provide new insight into changes in snowpack extremes, suggesting that bivariate or multivariate analysis of snowpack extremes should be a crucial focus of future studies.

Generally, snowpack extremes had a significant impact on warm-season compound hydroclimatic extremes, with the impact concentrated in the first three months after snowpack disappearance. Compared with compound hot-wet and cold-dry extremes, compound hot-dry and cold-wet extremes were more relevant to the corresponding snowpack extremes, largely owing to the low variability of the rich-short and deficient-long snowpack extremes. More importantly, comparisons of different snowpack extremes revealed that the combined impact of extreme changes in snowpack mass and duration surpassed that of individual snowpack characteristics, both in terms of spatial extent (>10%) and coincidence rate (>0.2). However, previous studies have extensively investigated the impacts[14,32–34] of snowpack changes, such as snow drought or extreme early snowmelt, based on a univariate framework. As snowpack extremes of lower mass tend to have a shorter duration, a univariate method might overlook the interaction of these variables and not fully capture their overall impact. In addition, the impact of the combined characteristics of snowpack was greater than that of the individual characteristics, for both individual (Supplementary Fig. 8) and compound hydroclimatic extremes. More comprehensive attribution studies are needed that consider the combined impact of different snowpack characteristics, rather than focus on a single aspect.

To clarify the cause-effect relations between snowpack extremes and compound hydroclimatic extremes, we examined the land surface and atmospheric conditions of the first snow-free month during the occurrence and non-occurrence of snowpack extremes, including soil moisture, surface sensible heat flux, evapotranspiration, and precipitation. These analyzed variables were closely linked to the impact of snowpack on energy and water cycle processes[35–37], which could reflect the main physical processes behind snowpack-compound hydroclimatic extremes relations. The results showed that when deficient-short snowpack extremes occurred, surface sensible heat generally increased, while soil moisture, evapotranspiration, and precipitation decreased (Supplementary Fig. 9). When rich-long snowpack extremes occurred, changes in these variables were reversed. We further explored whether the occurrence of current compound hydroclimatic extremes correlates with antecedent hydroclimatic conditions (1–3 months prior), and found that the impact of short-term antecedent hydroclimatic conditions was relatively weak (Supplementary Fig. 10).

These findings indicated an underlying mechanism that snowpack extremes could alter land surface and atmospheric hydrothermal conditions, thereby exerting an important role in subsequent compound hydroclimatic extremes after snowpack disappearance (Fig. 5). For example, deficient-short snowpack extremes generally decreased soil moisture and surface albedo, and increased surface sensible heat (increasing net solar radiation), which directly contributed to increasing air temperature and soil drought conditions and thus increased compound hot-dry extremes[38,39].

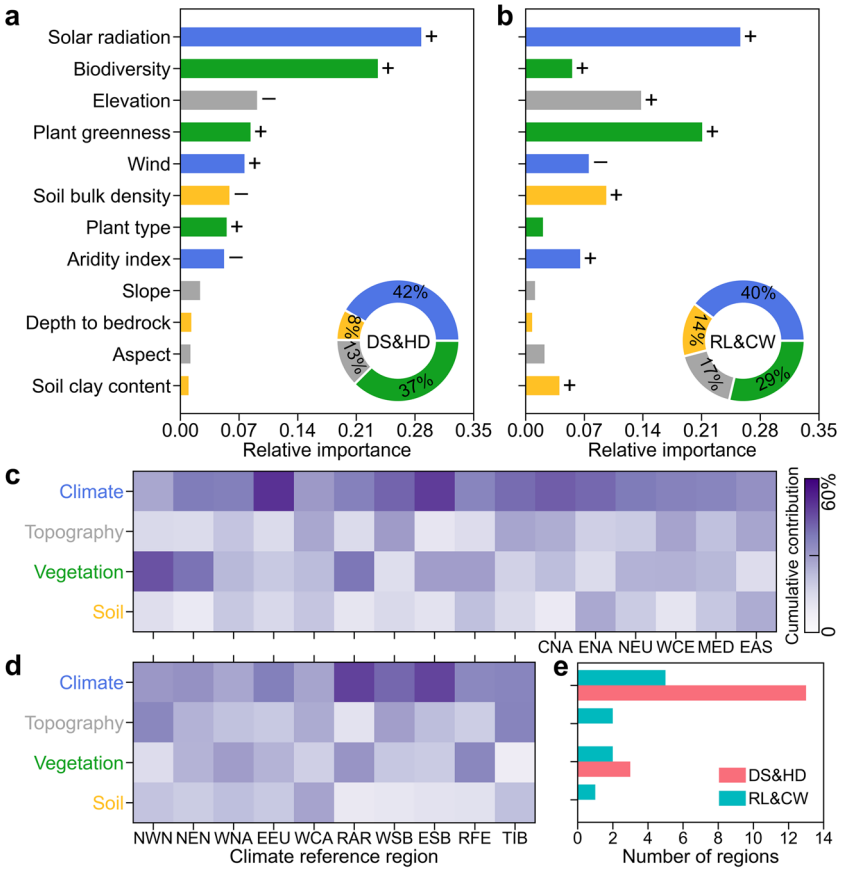

Fig. 4 | Contributions of four types of environmental factors to the hydroclimatic impact of snowpack extremes. a, **b** Relative importance of different variables for changes in the coincidence rate between deficient-short snowpack extremes and compound hot-dry extremes (DS&HD) (**a**) and between rich-long snowpack extremes and compound cold-wet extremes (RL&CW) (**b**). The inset circles of the bar plot indicate the cumulative contribution of four types of factors across the whole region. The "+" and "−" symbols in the bar plot indicate the significant positive and negative correlation between the variable and the coincidence rate, respectively, based on the partial contribution analysis. **c**, **d** Cumulative contributions of four types of factors to changes in coincidence rates of DS&HD and RL&CW events in different climate reference regions. Only regions with over 100 significant pixels are analyzed. **e** Number of climate reference regions affected by each dominant factor.

Meanwhile, low soil moisture usually reduces the evaporative cooling effect, and low surface latent heat suppresses the development of clouds and subsequent precipitation, consequently exacerbating the occurrence of compound hot-dry extremes. In addition to local effects, these physical processes might operate as teleconnections between different regions[40]. Moreover, snowpack extremes affect atmospheric circulation, such as geopotential height[41] and planetary waves[42], which are responsible for the development of compound hydroclimatic extremes.

Moreover, we found that shifts in environmental factors significantly influenced the hydroclimatic impacts of snowpack extremes (Fig. 4). By analyzing the annual trends of the four most significant environmental factors over the last four decades, we observed that changes in most factors have increasingly amplified differences in the hydroclimatic impact between deficient-short and rich-long snowpack extremes (Supplementary Table 2). Compared with changes in the occurrence probability of snowpack extremes, compound hydroclimatic extremes were more sensitive to changes in the intensity of snowpack extremes. As such, we suggest that intensity changes can be used as an effective new metric to improve the prediction of early compound hydroclimatic extremes. Recent studies have reported that snowpack in most regions will decrease in the future under different emission pathways[4,18,43]. Under this case, future DS&HD events are expected to occur more frequently, and the corresponding intensity is also projected to increase significantly. Consequently, the emerging consecutive extremes will have severe hydroclimatic and ecological consequences in snow-dependent regions, such as reduced freshwater availability[44], reduced crop yields[45], increased wildfires[46], and reduced vegetation productivity[23].

Several uncertainties in our study warrant mention, particularly in two aspects. First, although the datasets employed are regarded as state-of-the-art and have shown high reliability in station observations, interpolation to a uniform spatial resolution inevitably introduces errors. For the analysis, we focused on snowpack-induced compound hydroclimatic extremes at the monthly scale and the applicability of the findings at other timescales, such as weekly, sub-seasonal, and annual scales, which may need to be further explored owing to differences in timescale effects. Moreover, several factors influencing the relations between snowpack extremes and compound hydroclimatic extremes were not considered, including the influence of natural climate variability, such as the El Niño-Southern Oscillation[29], Atlantic Multidecadal Variability[47], and Pacific decadal oscillation[48]. The causal relations behind the observed patterns were also affected by non-local effects[49], and whether there was a bidirectional effect was completely unexamined[50]. Nevertheless, it is not possible in this study to analyze these impacts comprehensively at hemisphere scales, highlighting the need for additional analysis. Furthermore, disentangling the complex interactions between snowpack extremes and compound hydroclimatic extremes requires more accurate land-atmosphere climate modeling and enhanced observational capabilities.

Conclusion

This study provided the first detailed assessment of the spatial extent, temporal scale, and magnitude of the relation between different snowpack extremes and compound hydroclimatic extremes in the Northern Hemisphere. The results showed that snowpack extremes play an important role in regulating early warm-season compound hydroclimatic extremes. Monitoring changes in snowpack extremes could act as a winter precursor signal, providing early warnings for compound hot-dry and cold-wet extremes, particularly regarding changes in the intensity of snowpack extremes. Moreover, understanding how contributing environmental factors vary from region to region could be beneficial for formulating region-specific strategies to adapt to climate change. These findings improve the understanding of where and when compound hydroclimatic extremes respond to snowpack extremes in the Northern Hemisphere, and future studies are needed to address the elevated risk arising from these increasingly successive extremes.

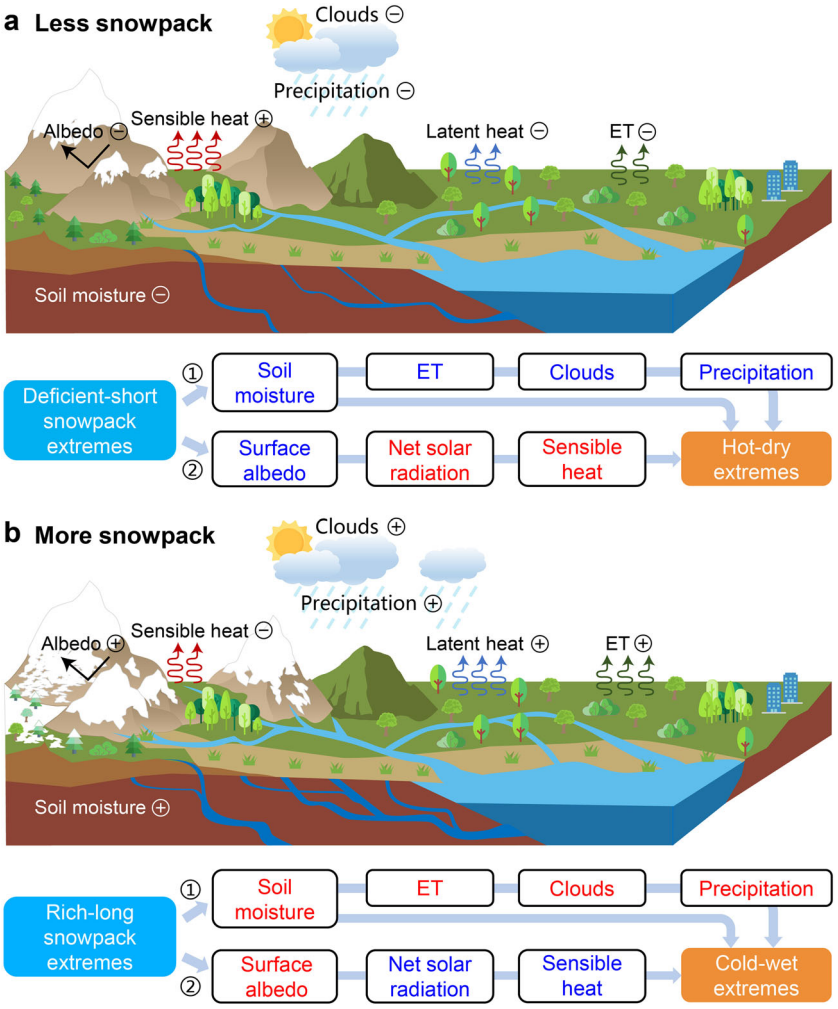

Fig. 5 | Schematic diagram illustrating the impact of snowpack extremes on land surface and atmospheric conditions. a Deficient-short snowpack extremes, meaning that less snowpack. **b** Rich-long snowpack extremes, meaning that more snowpack. The symbols "⊕" and "⊖" indicate increasing and deceasing changes in variables, respectively. The two main pathways (or effects) of snowpack extremes on compound hot-dry and cold-wet extremes are identified by altering soil moisture (① water availability process) and surface albedo (② radiative process) conditions. The red and blue text in the path diagram indicate increasing and decreasing changes in variables, respectively. ET, evapotranspiration.

Materials and methods

Observational datasets

We utilized three primary types of meteorological data from 1980 to 2022 in this study: snow water equivalent (SWE), air temperature, and soil moisture data. Considering the spatial domain (0–90°N) and fine spatiotemporal resolution for examining changes in snowpack extremes, the most advanced ERA5-Land reanalysis product was selected for analysis[51]. Additionally, we evaluated the accuracy of the daily ERA5-Land SWE data with available ground observations and found that it performed well and was more reliable than three other well-known SWE products, GlobSnow[52], Snow-CCI[53], and GLDAS[54] (Supplementary Fig. 11). Air temperature and soil moisture data were also derived from the ERA5-Land product and aligned well with ground observations and other common products, making them widely used in climate change studies[51,55]. We then used the monthly maximum SWE, maximum air temperature and four layers (0–289 cm) of mean soil moisture data to calculate the standardized SWE index (SWEI)[45], air temperature index (SATI), and soil moisture index (SSMI)[56], respectively. Moreover, daily SWE data were used to calculate the snowpack duration (for calculations, see supplementary methods S1) of a hydrological year (from 1 September to 30 June of the following year) and subsequently calculate the standardized snowpack duration index (SDI).

In addition, several types of auxiliary environmental data (climate, soil, topography, and vegetation factors) were collected to analyze the drivers of relations between snowpack extremes and compound hydroclimatic extremes. The annual mean aridity index was acquired from the global aridity and potential evapotranspiration map[57], and the annual mean wind and solar shortwave radiation data were calculated based on the ERA5-Land product. The soil property data (soil bulk density, soil clay content, and depth to bedrock) were acquired from the SoilGrids dataset[58]. The elevation data were obtained from the Global Multi-resolution Terrain Elevation Data 2010[59]. The plant greenness, characterized by the normalized difference vegetation index (NDVI), was extracted from the PKU GIMMS NDVI dataset[60]. The biodiversity and plant type data were obtained from global plant species[61] and ESA CCI land cover maps[62], respectively. All the datasets were aggregated to a spatial resolution of 0.25° × 0.25° before further analysis, and seasonal snow-dominated regions with snowpack duration ranging from 60 to 300 days were analyzed.

Identification and characterization of snowpack extremes

We defined eight types of snowpack extremes to assess changes in snowpack characteristics (mass and duration): rich, deficient, long, short, rich-long, rich-short, deficient-long, and deficient-short snowpack extremes (Table 1). The snowpack extremes were identified by annual SWEI and SDI values for each pixel. Following methodologies from previous studies[43,45], these values were calculated by the empirical probability via the inverse normal transformation. The empirical probability was derived from the nonparametric gringorten plotting position function $P = (i - 0.44)/(n + 0.12)$ (n: the sample size of the data; i: the rank of the nonzero variable). The SWEI from the month before snowpack end date was chosen to indicate the accumulated mass of snowpack during a hydrological year[14]. Note that thresholds of 0.8/−0.8 were selected to ensure a sufficient number of events for a reliable estimation of copula function parameters, as referenced in previous studies[63,64].

Table 1 | Characteristics and definitions of the eight types of snowpack extremes

Snowpack extremes type	Characteristic		Definition
	Mass	Duration	
Rich	▲	—	SWEI ≥ 0.8 ∩ −0.8 < SDI < 0.8
Deficient	▼	—	SWEI ≤ −0.8 ∩ −0.8 < SDI < 0.8
Long	—	▲	−0.8 < SWEI < 0.8 ∩ SDI ≥ 0.8
Short	—	▼	−0.8 < SWEI < 0.8 ∩ SDI ≤ −0.8
Rich-Long	▲	▲	SWEI ≥ 0.8 ∩ SDI ≥ 0.8
Rich-Short	▲	▼	SWEI ≥ 0.8 ∩ SDI ≤ −0.8
Deficient-Long	▼	▲	SWEI ≤ −0.8 ∩ SDI ≥ 0.8
Deficient-Short	▼	▼	SWEI ≤ −0.8 ∩ SDI ≤ −0.8

Note: ▲, ▼, and — indicate extremely high, extremely low, and normal values, respectively.

Following the calculations of the SWEI and SDI time series (1980–2022), we used the bivariate copula function to quantify the joint occurrence probability of snowpack extremes for each pixel (Supplementary Fig. 1), which has been widely applied to characterize the dependence between two variables, especially in a few samples[25]. Taking rich and deficient-long snowpack extremes as examples (others listed in Supplementary Table 1), the joint occurrence probability (P) can be given as follows:

$$\text{Rich: } P(u_1 \le SWEI \cap v_0 < SDI < v_1) = v_1 - v_0 + C(u_1, v_0) - C(u_1, v_1) \quad (1)$$

$$\text{Deficient} - \text{Long: } P(SWEI \le u_0 \cap SDI > v_1) = u_0 - C(u_o, v_1) \quad (2)$$

where C is a joint cumulative distribution function; u and v are the marginal cumulative distribution functions of the SWEI and SDI, respectively; and u_1/v_1 and v_0/v_0 are the marginal probabilities of SWEI/SDI above 0.8 and below −0.8, respectively. Five popular copula functions (independent, Gaussian, Clayton, Frank, and Gumbel)[65] were applied to link the marginal distributions of the SWEI and SDI. The Akaike information criterion[66] and root mean square error were used to determine the optimal fitting copula function.

Then, we analyzed the spatiotemporal dynamics of the occurrence probability and intensity of different snowpack extremes for each pixel with a 15-year moving window using the Theil-Sen[67] and Mann-Kendall trend[68] methods. The intensity of individual and compound snowpack extremes (i.e. rich-long, rich-short, deficient-long, and deficient-short) was determined by the absolute values of the SWEI or SDI and their combined products. In addition, 13-year and 17-year moving windows were used to examine the robustness of the temporal results.

Coincidence analysis of snowpack extremes and compound hydroclimatic extremes

We investigated the impact of eight types of snowpack extremes on four compound warm-season hydroclimatic extremes (hot-dry, hot-wet, cold-dry, and cold-wet). These hydroclimatic extremes were identified by the monthly SATI and SSMI, which were calculated in the same way as the SWEI. Next, we quantified the trigger coincidence rate between snowpack extremes and compound hydroclimatic extremes for each pixel via the event coincidence analysis method[69,70]. The coincidence rate (r) was calculated as the ratio of the number of coincidences of snowpack extremes followed by compound hydroclimatic extremes, expressed as:

$$r(\triangle T, \tau) = \frac{1}{N_{snow}} \sum_{i=1}^{N_{snow}} \Theta \left[\sum_{j=1}^{N_{hydro}} 1_{[0,\triangle T]} \left(\left(t_j^{hydro} - \tau \right) - t_i^{snow} \right) \right] \quad 0 \le r \le 1 \quad (3)$$

where N_{snow} and N_{hydro} are the total number of snowpack extremes and hydroclimatic extremes, respectively; Θ is a Heaviside function, defined as $\Theta(x) = 0$ for $x \le 0$ and $\Theta(x) = 1$ otherwise. $1_{[0,\triangle T]}$ is an indicator function of temporal tolerance $\triangle t$, defined as $1_{[0,\triangle T]}(x) = 1$ for $x \le \triangle t$ and $1_{[0,\triangle T]} = 0$ otherwise; here, $\triangle t$ is set to 0, and t_i^{snow} and t_j^{hydro} are the time series of snowpack extremes and hydroclimatic extremes, respectively. τ is the time lag parameter and represents the event at $(t_j^{hydro} - \tau) - t_i^{snow} \le \triangle T$.

A higher coincidence rate represents a greater impact of snowpack extremes on hydroclimatic extremes. Considering the temporal effect of snowpack extremes, we selected five potential impact lags, namely, 1–5 months after snowpack end date, for analysis within a year rather than across interannual years. Moreover, a shuffling test was conducted to examine the significance of the coincidence rate between snowpack extremes and hydroclimatic extremes. We shuffled the time series of snowpack extremes randomly while maintaining the sequence of compound hydroclimatic extremes. This process was repeated 1000 times to calculate the coincidence rate between snowpack extremes and compound hydroclimatic extremes in a randomly generated time series. A significant result was determined if the observed coincidence rate exceeded 95% of the 1000 random time series ($p < 0.05$). Only significant results were considered for the coincident analysis.

Furthermore, we designed a statistical framework to evaluate the distance scale of the spatial co-occurrence rate of snowpack-induced hydroclimatic extremes. Specifically, we first correlated snowpack extremes in a target pixel with hydroclimatic extremes of all other pixels in the study area and identified those with significant coincidence rates. Second, we compared the magnitude of all the candidate significant coincidence rates and determined the distance to the maximum coincidence rate as the distance scale of the spatial co-occurrence rate.

Importance of background environmental factors to snowpack-induced hydroclimatic extremes

The geographical detector model (GMD) was applied to determine the impact of four types of background environmental factors on changes in the coincidence rate of snowpack extremes with hydroclimatic extremes, including climate, soil, topography, and vegetation factors. Specifically, we extracted the annual mean aridity index, mean solar radiation, and mean wind, which were directly related to water and energy cycle processes, as climate factors. For soil factors, we considered soil properties such as soil bulk density, soil clay content, and depth to bedrock since they were closely linked to soil water redistribution[71] (e.g. infiltration). Topography factors including elevation, slope, and aspect were considered since they could significantly affect distribution patterns of climate variables such as snowpack[72] and precipitation[73]. The vegetation factors included the growing season NDVI, biodiversity, and plant type. These three variables were widely used as proxies of the impact of vegetation on hydroclimatic conditions such as soil moisture[40] and temperature[74].

The basic assumption of GMD method is that if a response variable significantly influences the explanatory variable, their spatial distributions will be similar, which is widely used to reveal spatial differentiation and driving factors[75,76]. Although GMD was not limited by multicollinearity of variables, we used the Variance Inflation Factor (VIF) to remove variables with high collinearity (VIF > 10, Supplementary Fig. 12), reducing their potential to obscure the ranking of variable importance. Then, we used the factor detection component of the geographic detector model to quantify the relative importance of explanatory variables based on the Q-statistic. The Q value of a response variable (Q_v) can be calculated as:

$$Q_v = 1 - \frac{\sum_{j=1}^{M} N_{v,j} \sigma_{v,j}^2}{N_v \sigma_v^2} \quad (4)$$

where N_v and σ_v^2 are the number and variance of samples in the entire study area of variable v, respectively; $N_{v,j}$ and $\sigma_{v,j}^2$ are the number and variance of samples in the jth ($j = 1, 2, \ldots, M$) sub-region of variable v, respectively.

The higher the significant Q value is (ranging from 0 to 1, $p < 0.05$, based on F-test), the greater the importance of the explanatory variable[77]. All the variable data were converted to categorical data before analysis, and the optimal discretization method was selected based on a set of supervised and unsupervised spacing classification methods (i.e. equal, natural, quantile, geometric, and standard deviation).

Data availability

All datasets used in this study are freely available online. ERA5-Land data are available at https://cds.climate.copernicus.eu/cdsapp#!/dataset/reanalysis-era5-land?tab=overview. The digital elevation data are available at https://www2.jpl.nasa.gov/srtm/. The plant greenness data are available at https://zenodo.org/record/7509116. Plant species data are available at https://databasin.org/datasets/43478f840ac84173979b22631c2ed672/.

Code availability

The processing codes for the analyses are available in a Zenodo repository at https://doi.org/10.5281/zenodo.13882068.

Received: 5 April 2024; Accepted: 26 September 2024;
Published online: 07 October 2024

References

1. Estilow, T. W., Young, A. H. & Robinson, D. A. A long-term Northern Hemisphere snow cover extent data record for climate studies and monitoring. *Earth Syst. Sci. Data* **7**, 137–142 (2015).
2. Pulliainen, J. et al. Patterns and trends of Northern Hemisphere snow mass from 1980 to 2018. *Nature* **581**, 294–298 (2020).
3. Kunkel, K. E. et al. Trends and Extremes in Northern Hemisphere Snow Characteristics. *Curr. Clim. Change Rep.* **2**, 65–73 (2016).
4. Zhu, X. et al. Historical evolution and future trend of Northern Hemisphere snow cover in CMIP5 and CMIP6 models. *Environ. Res. Lett.* **16**, 065013 (2021).
5. Hale, K. E., Jennings, K. S., Musselman, K. N., Livneh, B. & Molotch, N. P. Recent decreases in snow water storage in western North America. *Commun. Earth Environ.* **4**, 1–11 (2023).
6. Mote, P. W. et al. Perspectives on the causes of exceptionally low 2015 snowpack in the western United States. *Geophys. Res. Lett*. **43** (2016).
7. Avanzi, F. et al. Winter snow deficit was a harbinger of summer 2022 socio-hydrologic drought in the Po Basin, Italy. *Commun. Earth Environ.* **5**, 1–12 (2024).
8. 'Snow droughts' followed by extreme heat are striking more of the planet. *Nature* **607**, 215–215 (2022).
9. Wu, Z., Zhang, P., Chen, H. & Li, Y. Can the Tibetan Plateau snow cover influence the interannual variations of Eurasian heat wave frequency? *Clim. Dyn.* **46**, 3405–3417 (2016).
10. Dierauer, J. R., Allen, D. M. & Whitfield, P. H. Snow drought risk and susceptibility in the western United States and southwestern Canada. *Water Resour. Res.* **55**, 3076–3091 (2019).
11. Velásquez, N., Quintero, F., Koya, S. R., Roy, T. & Mantilla, R. Snow-detonated floods: Assessment of the U.S. midwest march 2019 event. *J. Hydrol. Reg. Stud.* **47**, 101387 (2023).
12. Flach, M. et al. Contrasting biosphere responses to hydrometeorological extremes: revisiting the 2010 western Russian heatwave. *Biogeosciences* **15**, 6067–6085 (2018).
13. IPCC, 2022: Climate Change 2022: Impacts, Adaptation, and Vulnerability. Contribution of Working Group II to the Sixth Assessment Report of the Intergovernmental Panel on Climate Change (eds. Pörtner, H.-O. et al.) 1–2275 (Cambridge University Press, 2022).
14. Li, X. & Wang, S. Recent increase in the occurrence of snow droughts followed by extreme heatwaves in a warmer world. *Geophys. Res. Lett.* **49**, e2022GL099925 (2022).
15. Harpold, A., Dettinger, M. & Rajagopal, S. Defining snow drought and why it matters. *Eos Trans. Am. Geophys. Union* https://doi.org/10.1029/2017EO068775 (2017).
16. Dierauer, J. R., Whitfield, P. H. & Allen, D. M. Climate controls on runoff and low flows in mountain catchments of Western North America. *Water Resour. Res.* **54**, 7495–7510 (2018).
17. Diffenbaugh, N. S., Scherer, M. & Ashfaq, M. Response of snow-dependent hydrologic extremes to continued global warming. *Nat. Clim. Change* **3**, 379–384 (2013).
18. Cho, E., McCrary, R. R. & Jacobs, J. M. Future changes in snowpack, snowmelt, and runoff potential extremes over North America. *Geophys. Res. Lett.* **48**, e2021GL094985 (2021).
19. Callaghan, T. V. et al. Multiple effects of changes in Arctic snow cover. *Ambio* **40**, 32–45 (2011).
20. Sun, P. et al. Compound and successive events of extreme precipitation and extreme runoff under heatwaves based on CMIP6 models. *Sci. Total Environ.* **878**, 162980 (2023).
21. Min, R., Gu, X., Guan, Y. & Zhang, X. Increasing likelihood of global compound hot-dry extremes from temperature and runoff during the past 120 years. *J. Hydrol.* **621**, 129553 (2023).
22. Ridder, N. N. et al. Global hotspots for the occurrence of compound events. *Nat. Commun.* **11**, 5956 (2020).
23. Yin, J. et al. Future socio-ecosystem productivity threatened by compound drought–heatwave events. *Nat. Sustain.* **6**, 259–272 (2023).
24. Wu, Y. et al. Effects of snow cover on spring vegetation phenology vary with temperature gradient across the Pan-Arctic. *J. Geophys. Res. Biogeosciences* **128**, e2022JG007183 (2023).
25. Zscheischler, J. & Seneviratne, S. I. Dependence of drivers affects risks associated with compound events. *Sci. Adv.* **3**, e1700263 (2017).
26. Bastos, A. et al. A joint framework for studying compound ecoclimatic events. *Nat. Rev. Earth Environ.* **4**, 333–350 (2023).
27. Kouki, K., Räisänen, P., Luojus, K., Luomaranta, A. & Riihelä, A. Evaluation of Northern Hemisphere snow water equivalent in CMIP6 models during 1982–2014. *The Cryosphere* **16**, 1007–1030 (2022).
28. Musselman, K. N., Addor, N., Vano, J. A. & Molotch, N. P. Winter melt trends portend widespread declines in snow water resources. *Nat. Clim. Change* **11**, 418–424 (2021).
29. Fang, Y. & Leung, L. R. Northern Hemisphere Snow Drought in Earth System Model Simulations and ERA5-Land Data in 1980–2014. *J. Geophys. Res. Atmos.* **128**, e2023JD039308 (2023).
30. Gottlieb, A. R. & Mankin, J. S. Evidence of human influence on Northern Hemisphere snow loss. *Nature* **625**, 293–300 (2024).
31. Mudryk, L. et al. Historical Northern Hemisphere snow cover trends and projected changes in the CMIP6 multi-model ensemble. *Cryosphere* **14**, 2495–2514 (2020).
32. Dong, W., Jia, X. & Wu, R. Impact of summer Tibetan Plateau snow cover on the variability of concurrent compound heatwaves in the Northern Hemisphere. *Environ. Res. Lett.* **19**, 014057 (2023).
33. Livneh, B. & Badger, A. M. Drought less predictable under declining future snowpack. *Nat. Clim. Change* **10**, 452–458 (2020).
34. Jenicek, M. & Ledvinka, O. Importance of snowmelt contribution to seasonal runoff and summer low flows in Czechia. *Hydrol. Earth Syst. Sci.* **24**, 3475–3491 (2020).
35. Flanner, M. G., Shell, K. M., Barlage, M., Perovich, D. K. & Tschudi, M. A. Radiative forcing and albedo feedback from the Northern Hemisphere cryosphere between 1979 and 2008. *Nat. Geosci.* **4**, 151–155 (2011).
36. Fyfe, J. C. et al. Large near-term projected snowpack loss over the western United States. *Nat. Commun.* **8**, 14996 (2017).

37. Dutra, E., Schär, C., Viterbo, P. & Miranda, P. M. A. Land-atmosphere coupling associated with snow cover. *Geophys. Res. Lett*. **38**, https://doi.org/10.1029/2011GL048435 (2011).
38. Flanner, M. G. et al. Springtime warming and reduced snow cover from carbonaceous particles. *Atmos. Chem. Phys.* **9**, 2481–2497 (2009).
39. Dirmeyer, P. A., Balsamo, G., Blyth, E. M., Morrison, R. & Cooper, H. M. Land-atmosphere interactions exacerbated the drought and heatwave over Northern Europe during summer 2018. *AGU Adv* **2**, e2020AV000283 (2021).
40. Lian, X. et al. Summer soil drying exacerbated by earlier spring greening of northern vegetation. *Sci. Adv.* **6**, eaax0255 (2020).
41. Li, W. et al. Influence of Tibetan Plateau snow cover on East Asian atmospheric circulation at medium-range time scales. *Nat. Commun.* **9**, 4243 (2018).
42. Dong, W., Jia, X. & Wu, R. Intensified impact of spring Tibetan Plateau snow cover on summer compound heat waves in Western Europe after 1998. *J. Clim.* **37**, 2423–2441 (2024).
43. Cowherd, M., Leung, L. R. & Girotto, M. Evolution of global snow drought characteristics from 1850 to 2100. *Environ. Res. Lett.* **18**, 064043 (2023).
44. Siirila-Woodburn, E. R. et al. A low-to-no snow future and its impacts on water resources in the western United States. *Nat. Rev. Earth Environ.* **2**, 800–819 (2021).
45. Huning, L. S. & AghaKouchak, A. Global snow drought hot spots and characteristics. *Proc. Natl. Acad. Sci.* **117**, 19753–19759 (2020).
46. Scholten, R. C., Coumou, D., Luo, F. & Veraverbeke, S. Early snowmelt and polar jet dynamics co-influence recent extreme Siberian fire seasons. *Science* **378**, 1005–1009 (2022).
47. Zampieri, M., Scoccimarro, E. & Gualdi, S. Atlantic influence on spring snowfall over the Alps in the past 150 years. *Environ. Res. Lett.* **8**, 034026 (2013).
48. Delworth, T. L., Zeng, F., Rosati, A., Vecchi, G. A. & Wittenberg, A. T. A link between the hiatus in global warming and North American drought. *J. Clim.* **28**, 3834–3845 (2015).
49. Yang, K., Qi, Q. & Wang, C. Possible impacts of vegetation cover increment on the relationship between winter snow cover anomalies over the Third Pole and summer precipitation in East Asia. *Npj Clim. Atmos. Sci.* **6**, 140 (2023).
50. Reyes, L. & Kramer, M. G. High-elevation snowpack loss during the 2021 Pacific Northwest heat dome amplified by successive spring heatwaves. *Npj Clim. Atmos. Sci.* **6**, 1–12 (2023).
51. Muñoz-Sabater, J. et al. ERA5-Land: a state-of-the-art global reanalysis dataset for land applications. *Earth Syst. Sci. Data* **13**, 4349–4383 (2021).
52. Luojus, K. et al. GlobSnow v3.0 Northern Hemisphere snow water equivalent dataset. *Sci. Data* **8**, 163 (2021).
53. Luojus, K. et al. ESA Snow Climate Change Initiative (Snow_cci): Snow Water Equivalent (SWE) level 3C daily global climate research data package (CRDP) (1979–2020), version 2.0. NERC EDS Centre for Environmental Data Analysis (2022) https://doi.org/10.5285/4647CC9AD3C044439D6C643208D3C494.
54. Rodell, M. et al. The global land data assimilation system. *Bull. Am. Meteorol. Soc.* **85**, 381–394 (2004).
55. Sheridan, S. C., Lee, C. C. & Smith, E. T. A comparison between station observations and reanalysis data in the identification of extreme temperature events. *Geophys. Res. Lett.* **47**, e2020GL088120 (2020).
56. Tabari, H. & Willems, P. Global risk assessment of compound hot-dry events in the context of future climate change and socioeconomic factors. *Npj Clim. Atmos. Sci.* **6**, 1–10 (2023).
57. Zomer, R. J., Xu, J. & Trabucco, A. Version 3 of the Global Aridity Index and Potential Evapotranspiration Database. *Sci. Data* **9**, 409 (2022).
58. Hengl, T. et al. SoilGrids250m: Global gridded soil information based on machine learning. *PLOS ONE* **12**, e0169748 (2017).
59. Danielson, J. J. & Gesch, D. B. Global multi-resolution terrain elevation data 2010 (GMTED2010) (2011).
60. Li, M. et al. Spatiotemporally consistent global dataset of the GIMMS Normalized Difference Vegetation Index (PKU GIMMS NDVI) from 1982 to 2022. *Earth Syst. Sci. Data* **15**, 4181–4203 (2023).
61. Kier, G. et al. Global patterns of plant diversity and floristic knowledge. *J. Biogeogr.* **32**, 1107–1116 (2005).
62. ESA. Land Cover CCI Product User Guide Version 2. Tech. Rep. Available at: maps.elie.ucl.ac.be/CCI/viewer/download/ESACCI-LC-Ph2-PUGv2_2.0.pdf. (2017).
63. Hao, Z. & AghaKouchak, A. A nonparametric multivariate multi-index drought monitoring framework. *J. Hydrometeorol.* **15**, 89–101 (2014).
64. Tabari, H. & Willems, P. Trivariate analysis of changes in drought characteristics in the CMIP6 multimodel ensemble at global warming levels of 1.5°, 2°, and 3 °C. *J. Clim.* **35**, 5823–5837 (2022).
65. Nelsen, R. B. *An Introduction to Copulas* (Springer Science & Business Media, 2007).
66. Akaike, H. A new look at the statistical model identification. *IEEE Trans. Autom. Control* **19**, 716–723 (1974).
67. Sen, P. K. Estimates of the regression coefficient based on Kendall's tau. *J. Am. Stat. Assoc.* **63**, 1379–1389 (1968).
68. Hamed, K. H. & Rao, A. R. A modified Mann-Kendall trend test for autocorrelated data. *J. Hydrol.* **204**, 182–196 (1998).
69. Donges, J. F., Schleussner, C.-F., Siegmund, J. F. & Donner, R. V. Event coincidence analysis for quantifying statistical interrelationships between event time series: on the role of flood events as triggers of epidemic outbreaks. *Eur. Phys. J. Spec. Top.* **225**, 471–487 (2016).
70. He, X. & Sheffield, J. Lagged compound occurrence of droughts and pluvials globally over the past seven decades. *Geophys. Res. Lett.* **47**, e2020GL087924 (2020).
71. Martínez-Fernández, J., González-Zamora, A. & Almendra-Martín, L. Soil moisture memory and soil properties: an analysis with the stored precipitation fraction. *J. Hydrol.* **593**, 125622 (2021).
72. Tennant, C. J. et al. Regional sensitivities of seasonal snowpack to elevation, aspect, and vegetation cover in western North America. *Water Resour. Res.* **53**, 6908–6926 (2017).
73. Saavedra, M., Junquas, C., Espinoza, J.-C. & Silva, Y. Impacts of topography and land use changes on the air surface temperature and precipitation over the central Peruvian Andes. *Atmospheric Res* **234**, 104711 (2020).
74. Zeng, Z. et al. Climate mitigation from vegetation biophysical feedbacks during the past three decades. *Nat. Clim. Change* **7**, 432–436 (2017).
75. Zhang, X. et al. Observed changes in extreme precipitation over the Tienshan Mountains and associated large-scale climate teleconnections. *J. Hydrol.* **606**, 127457 (2022).
76. Wang, J. F. & Xu, C. Geodetector: principle and prospective. *Acta Geogr Sin* **72**, 116–134 (2017).
77. Song, Y., Wang, J., Ge, Y. & Xu, C. An optimal parameters-based geographical detector model enhances geographic characteristics of explanatory variables for spatial heterogeneity analysis: cases with different types of spatial data. *GIScience Remote Sens.* **57**, 593–610 (2020).
78. Iturbide, M. et al. An update of IPCC climate reference regions for subcontinental analysis of climate model data: definition and aggregated datasets. *Earth Syst. Sci. Data* **12**, 2959–2970 (2020).

Acknowledgements

This work was supported by the National Natural Science Foundation of China (Grant No. 42171307) and the "GeoX" Interdisciplinary Research Funds for the Frontiers Science Center for Critical Earth Material Cycling,

Nanjing University. We also thank the High-Performance Computing Center, Nanjing University, for computational support.

Author contributions

H.L., P.X., and X.Z. conceived and designed the study. H.L. conducted the analysis and drafted the manuscript. Y.L., B.T., S.C., and Y.L. collected and processed datasets. All authors participated in interpreting the results and revising the manuscript.

Competing interests

The authors declare no competing interests.

Additional information

Supplementary information The online version contains supplementary material available at https://doi.org/10.1038/s43247-024-01734-8.

Correspondence and requests for materials should be addressed to Pengfeng Xiao.

Peer review information *Communications Earth & Environment* thanks Ryan Webb and the other, anonymous, reviewer(s) for their contribution to the peer review of this work. Primary Handling Editor: Alireza Bahadori. A peer review file is available